Chinese Journal of Physics 72 (2021) 223–228

Contents lists available at ScienceDirect

Chinese Journal of Physics

journal homepage: www.sciencedirect.com/journal/chinese-journal-of-physics

Resistivity superconducting transition in single-crystalline $Cd_{0.95}Ni_{0.05}Sb$ system consisting of non-superconducting CdSb and NiSb phases

Oleg Ivanov [a,b,*], Vasily Zakhvalinskii [b], Evgeny Pilyuk [b], Aleksey Kochura [c], Aleksandr Kuz'menko [c], Aleksey Ril' [d]

[a] Belgorod State University, Belgorod 308015, Russian Federation
[b] Belgorod State Technological University named after V.G. Shukhov, Belgorod 308012, Russian Federation
[c] Southwest State University, Kursk 305040, Russian Federation
[d] Kurnakov Institute of General and Inorganic Chemistry, Russian Academy of Sciences, Moscow 119991, Russian Federation

ARTICLE INFO

Keywords:
Two-component CdSb - NiSb system
Inhomogeneous conducting systems
Electrical properties
Superconductivity
Hopping conductivity

ABSTRACT

Resistivity superconducting transition has been for the first time found in single crystal of two-component 0.95(CdSb)–0.05(NiSb) system. End members of the system are not superconductors under normal conditions. Insulating behavior in temperature dependence of the electrical resistivity, which is due to hopping conductivity, precedes the transition. The resistivity superconducting transition is rather broad, since at cooling down the electrical resistivity starts to fall at 10.5 K, whereas zero resistivity is reached only at ~2.3 K. Longitudinal magnetic field gradually depresses superconductivity and shifts the superconducting transition to lower temperatures. Under magnetic field above 0.5 T, superconductivity is totally destroyed. Main features observed in the resistivity superconducting transition, including its unusually big width and insulating electrical behavior above the transition, can be related to inhomogeneity of the single crystal studied. According to XRD and SEM examinations, the single crystal consists of major CdSb phase and minor NiSb phase. The NiSb phase forms inhomogeneities in the CdSb matrix. Micro-sized needle-like NiSb crystals and nano-sized $Ni_{1-x}Sb_x$ clusters can be considered as typical inhomogeneities.

1. Introduction

Forming inhomogeneous and disordered structures in solids is usually applied as a fruitful way to tune their properties in a desired manner. Inhomogeneous and disordered conductors and semiconductors often demonstrate unusual and specific features in behavior of their electrical properties, which are related to developing new mechanisms of conductivity and magnetoresistance [1-7], forming unstable and metastable states [8-10], arising strong fluctuation corrections to conductivity, which affect a superconducting transition [11-15], and etc. All the features in the electrical properties are dominantly originated from compositional and phase inhomogeneity, and structural disorder. There are many ways to prepare inhomogeneous and disordered solid-state systems. One of ways is based on applying two-component systems, in which components are characterized by a limited solubility and can form eutectic alloys [16-18].

* Corresponding author.
E-mail address: Ivanov.Oleg@bsu.edu.ru (O. Ivanov).

https://doi.org/10.1016/j.cjph.2021.05.004
Received 9 December 2020; Received in revised form 16 February 2021; Accepted 5 May 2021
Available online 13 May 2021

At high temperatures above a melting point, these systems are homogeneous. During solidification, initial homogeneity starts destroying, and two individual phases corresponding to components of system are gradually formed. Morphology, microstructure, phase and elemental composition of the solidified material are strongly dependent on a ratio between components and conditions of the solidification. Two-component CdSb–NiSb system is excellent example of the systems with limited solubility of components, which can be applied to prepare strongly inhomogeneous and disordered single-crystalline samples [19]. Two types of inhomogeneities can be considered in samples of this system, prepared via the solidification. Micro-sized needle-like NiSb crystals are the first type, whereas nano-sized $Ni_{1-x}Sb_x$ clusters are the second type. Both needle-like crystals and nano-clusters are distributed inside CdSb matrix.

In this paper, the electrical properties of single-crystalline $Cd_{0.95}Ni_{0.05}Sb$ system are examined within broad temperature interval. A few unusual features in these properties were found. The most intrigue feature is finding resistivity superconducting transition.

2. Materials and methods

Single crystal being studied was grown by the Bridgman method, which is based on slow cooling of a melt under temperature gradient. Two-stage process was applied. At the first stage, Ni was dissolved in Cd melt at temperature of 700 °C for 8 h. At the second stage, stoichiometric amounts of Sb and Cd:Ni powders corresponding to $Cd_{0.95}Ni_{0.05}Sb$ composition were loaded into a quartz ampoule covered with thin graphite layer and filled after evacuation with Ar gas to $p = 0.1$ atm. After holding the ampoule at temperature of 460 °C for 12 h, it was cooled down at a rate of 0.5 °C·h^{-1}.

XRD (X-ray diffraction) analysis of the single crystal was carried out by a Bruker D8 Advance diffractometer. Scanning electron microscopy (SEM) was involved to examine surface morphology of the crystal. Real elemental composition of the crystal was determined by energy dispersive X-ray spectroscopy (EDXS) method. To measure the specific electrical resistivity, ρ, a Mini Cryogen Free Measurements System was applied. The ρ measurements were carried out by four-probe method with reversing measuring current.

3. Results and discussion

To determine phase composition of the crystal, XRD analysis of powder, prepared by grinding the crystal, was carried out. The single crystal consisted of two phases (Fig. 1). Major phase is orthorhombic *Pbca* phase characteristic for CdSb (lattice parameters are $a = 0.6469(1)$ nm, $b = 0.8251(2)$ nm and $c = 0.8522(2)$ nm), whereas minor phase is hexagonal $P6_3/mmc$ phase characteristic for NiSb (lattice parameters are $a = b = 0.3923$ nm and $c = 0.5132$ nm). Two phases are observed in SEM-image taken from surface, which is oriented parallel to crystal (001) plane (inset to Fig. 1). Minor NiSb phase is formed as a system of needle-like crystals with length up to ~50 μm and width of 1–3 μm, which are distributed over CdSb surface (major phase). Real elemental composition of two phases, which was determined by EDXS method, is slightly deviated from ideal CdSb and NiSb compositions (Table 1). Actually, Ni partially substitutes for Cd in CdSb, and Cd partially substitutes for Ni in NiSb. These substitutions resulted from high-temperature diffusion redistribution of the elements, which occurred during growth of the single crystal.

Plate-like rectangular sample with dimensions of $4.25 \times 1.95 \times 0.78$ mm^3 was used to measure ρ. In accordance with results of high-resolution X-ray diffraction analysis performing the Bragg-Brentano method, the single crystal being studied was mosaic one and consisted of many blocks, which are slightly disoriented relative to each other, and with sizes of several dozens of micrometers. Detailed analysis of the block microstructure will be reported elsewhere. The blocks are partially ordered with preferential crystalline orientation. For the rectangular sample, its larger surface corresponded to preferential orientating the blocks with crystal (001) plane,

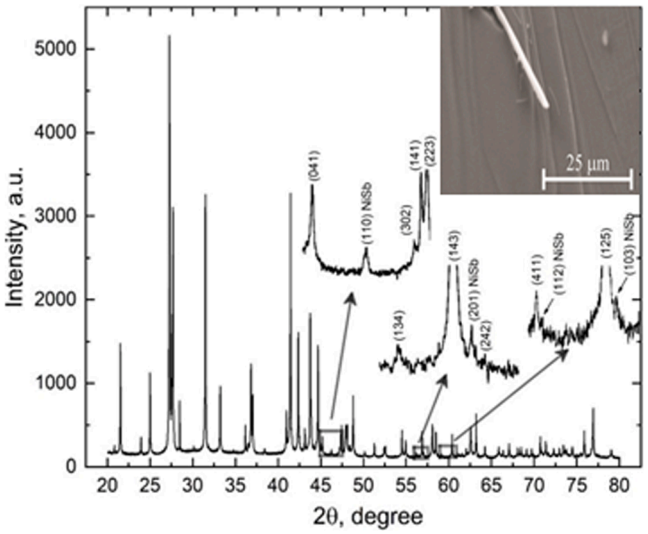

Fig. 1. XRD-pattern of powder prepared by grinding the single crystal with nominal $Cd_{0.95}Ni_{0.05}Sb$ composition. Inset is SEM-image taken from surface, oriented parallel to crystal (100) plane.

Table 1
Elemental composition for surface and needle-like crystals.

Element	Concentrations for surface [at.%]	Concentrations for needle-like crystals [at.%]
Cd	49.4	0.8
Ni	0.5	46.1
Sb	50.1	53.1

and the needle-like NiSb crystals were oriented parallel to long side of the rectangular.

The $\rho(T)$ dependence taken for 1.6–200 K interval is presented in Fig. 2. This dependence can be divided into three parts. At cooling from 200 K down to $T_{MI}\approx$45 K (part I), ρ is steady decreasing. This $\rho(T)$ behavior is characteristic of metal. At further cooling between T_{MI} and $T_m\approx$10.5 K (part II), ρ is increasing that corresponds to insulating behavior. So, a metal-insulator transition occurs at T_{MI}. Below T_m (part III), ρ starts to fall reaching zero value at $T_{C0}\approx$2.3 K. This feature in the resistivity can be related to a superconducting transition. Therefore, the resistivity superconducting transition occurs in the single crystal being studied. The metal $\rho(T)$ behavior (part I) should be attributed to acoustic phonon scattering of electrons. The $\mu(T)$ dependence due this scattering is expressed as [2]

$$\mu = \frac{2\sqrt{2\pi}\, e\hbar^2 d v_s^2}{3m^{*5/2}(kT)^{3/2}D_{ac}^2}, \tag{1}$$

where $\hbar$ is Plank constant, e is unit charge, d is mass density, υ_s is sound velocity, m^* is density-of-states effective mass, k is Boltzmann constant and D_{ac} is deformation potential.

In accordance with expression (1) and taking into account $\mu\sim\rho^{-1}$ link, the experimental $\rho(T)$ dependence was replotted to ρ–$T^{3/2}$ coordinates, as is shown in lower inset to Fig. 2. The replotted dependence is linear. Therefore, expression (1) very well fits the experimental $\rho(T)$ curve above T_{MI}.

To describe the insulating $\rho(T)$ behavior (part II), expression corresponding to hopping conductivity mechanism was applied as follows [1]

$$\rho \sim exp\left[\left(\frac{T_0}{T}\right)\right]^{1/2}, \tag{2}$$

where T_0 is characteristic temperature depending on particular microscopic characteristics of material.

In accordance with expression (2), the $\rho(T)$ dependence taken between the T_{MI} and T_m temperatures was replotted to $\ln\rho$–$T^{-1/2}$ coordinates, as is shown in upper inset to Fig. 2. For temperatures somewhat distant from T_{MI} and T_m, the replotted dependence is linear. Therefore, expression (2) can be really applied to fit the experimental $\rho(T)$ curve.

A few features of the resistivity superconducting transition were found. Firstly, the transition is broad with transition width equal to ΔT=T_m–$T_{C0}\approx$8.2 K. Secondly, the transition is implemented as the insulator-superconductor transition, since the insulating $\rho(T)$ behavior is observed above the transition. Finally, another feature was extracted from examination of longitudinal magnetic field effect on the transition. The $\rho(T)$ dependences taken for various magnetic fields with induction B = 0.00, 0.05, 0.15, 0.25 and 0.50 T are shown in Fig. 3. The transition is shifted to lower temperatures under magnetic field. Even under weakest field of 0.05 T, a superconducting state with zero electric resistivity is already not formed, i.e. the sample is in a resistivity state down to lowest

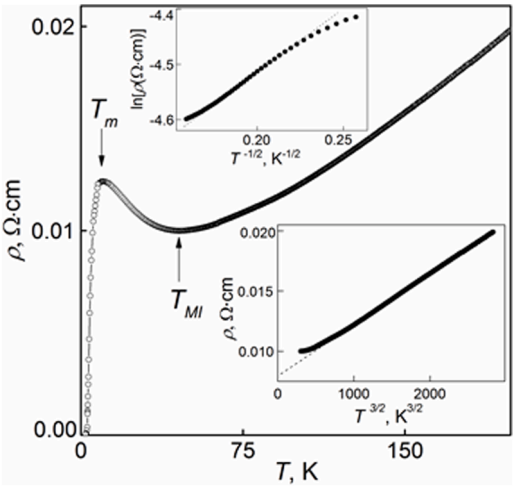

Fig. 2. The $\rho(T)$ dependence taken at zero magnetic field within broad temperature interval. Upper inset is the $\ln\rho(T^{-1/2})$ dependence, related to hopping conductivity (between T_{MI} and T_C); lower inset is the $\rho(T^{3/2})$ dependence, related to acoustic phonon scattering (above T_{MI}).

temperature of 1.6 K. Resistivity value at 1.6 K is steady increasing with increasing B, i.e. the resistivity state is stabilized under magnetic field. At $B \geq 0.5$ T, the $\rho(T)$ dependences are B–independent, since the $\rho(T)$ curves for these magnetic fields coincide with each other. A few kinks are observed in the $\rho(T)$ curves at temperatures T_i, and temperature position of these kinks is B – dependent. Thus, longitudinal magnetic field depresses the superconducting transition at $0 \leq B < 0.5$ T up to total destroying the superconducting state at $B \geq 0.5$ T. Temperature T_m is B-independent. The $\rho(T)$ maximum is also observed for $B \geq 0.5$ T, when the superconducting transition is totally depressed. This destroying the superconducting state can be characterized by analyzing the $\rho(B)$ curves, taken at temperatures below T_c. The $\rho(B)$ curves taken at 1.6, 4.0 and 7.0 K are shown in Fig. 4. The superconducting state is destroyed within broad range of magnetic fields in rather complicated manner that is characteristic of type-II superconductors. Similarly to the $\rho(T)$ dependences (Fig. 2), kinks in the $\rho(B)$ curves can be also observed at fields, designated as B_i in Fig. 2. Critical magnetic field, which corresponds to total destroying the superconducting state, is designated as B_C. Above B_C, the electrical resistivity is very weak B–dependent. The field B_C is gradually decreasing with increasing temperature, tending to zero at $T_C \approx 8$ K. The temperature T_C corresponds to temperature of the superconducting transition onset.

The features of the superconducting transition found in single-crystalline $Cd_{0.95}Ni_{0.05}Sb$ system are characteristic for granular conductor systems [13]. These systems are typical example of inhomogeneous and disordered systems. Ideally, they consist of close-packed metallic granules possessing high enough conductivity, which are separated by intergranular insulating boundaries. The superconducting transition observed in granular conducting systems is really broad. Broadening the transition is related to several mechanisms, as follows:

(A) Temperature of the superconducting transition in granular systems is dependent on granule size, r, in accordance with expression [20]

$$\frac{T_C}{T_{CB}} = \frac{1}{1+0.674(a_0/r)} \times exp\left[\frac{1.04(1+\lambda^b)}{\lambda^b - 0.1(1+\lambda^b)} - \frac{1.04(1+k\lambda^b)}{k\lambda^b - 0.1(1+0.63k\lambda^b)}\right],\ k = \frac{1+0.674(a_0/r)}{1-0.551(a_0/r)}, \tag{3}$$

where a_0 is interatomic distance, λ^b is electron-phonon coupling constant for bulk metal, and T_{CB} is temperature of the superconducting transition in bulk metal, but which is granular material in relevant granular system.

According to expression (3), T_C enhances with increasing r, and this tendency becomes more expressed for nano-sized granules. The r-effect on T_C is originated from large surface-to-volume ratio characteristic for metallic granules, separated by insulating boundaries, which results in enhancing electron-phonon coupling constant through softening phonon mode. If granule size is distributed within broad range, the superconducting transition will be rather broad, too, since granules with different size will undergo a local superconducting transition at strongly defined temperature.

(B) The superconducting transition in granular conducting system is usually two-staged [21]. Under cooling down the sample through the superconducting transition, each of individual granules gradually becomes superconducting, but coherent superconducting state within of total volume of the sample is not yet formed (at the first stage). At lower temperatures, all superconducting granules are already coupled, i.e. coherent superconducting state within of total volume is formed (at the second stage). Implementation of the superconducting transition through two stages also results in broadening the transition.

(C) Broadening the superconducting transition can be attributed to fluctuation conductivity [13]. Generally, corrections to the conductivity, which are related to superconducting fluctuations, include correction to the conductivity via reduction in density of states due to forming virtual Cooper pairs (DOS), and Aslamazov-Larkin (AL) and Maki-Thompson (MT) contributions to the conductivity. The AL contribution is due to forming non-equilibrium Cooper pairs above temperature of the superconducting transition, which results in new contribution to charge transfer. The MT contribution is related to coherent scattering of electrons, which form the Cooper pairs on impurities.

Let us discuss the insulating $\rho(T)$ behavior, which is observed above the superconducting transition. Depending on intergranular coupling strength, granular conductor system can behave either metal or insulator [13]. If the coupling between granules is sufficiently strong, granular system will be well conducting. In case of low coupling, granular system will behave as insulator. In the last case, the insulator-superconductor transition can take place at low temperatures. Expression (2) was firstly developed for heavily doped

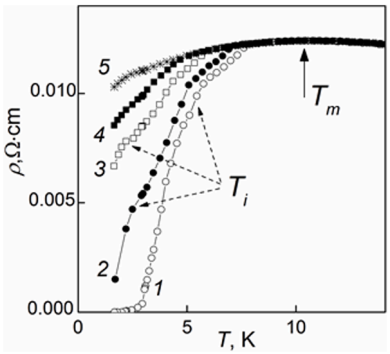

Fig. 3. The $\rho(T)$ dependences taken at magnetic fields of 0.00 (curve *1*), 0.05 (*2*), 0.15 (*3*), 0.25 (*4*) and 0.50 T (*5*).

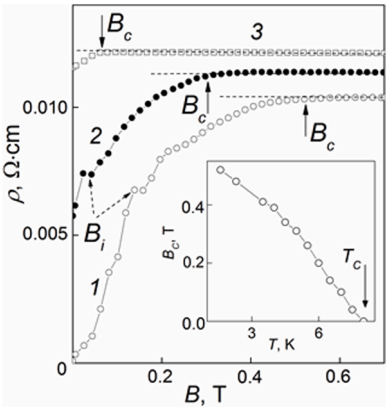

Fig. 4. The $\rho(B)$ dependences taken at temperatures of 1.6 (curve *1*), 4.0 (*2*) and 7.0 K (*3*). Inset is the $B_c(T)$ dependence.

semiconductors [1]. For these semiconductors, expression (2) corresponds to variable-range hopping conductivity. Hopping conductivity is related to tunneling of electron from one to another localized state within impurity energy band. Unit tunneling process is considered as electron hop. Besides heavily doped semiconductors, expression (2) can be also applied to describe the insulating $\rho(T)$ behavior in granular conducting systems [13]. For these systems, electron transport takes place as tunneling of electron through potential barriers, associated with intergranular contacts. Hopping processes in granular conducting systems is similar to hopping conductivity in heavily doped semiconductors. Both hopping conductivities are implemented in the same manner and described by the same expression. In heavily doped semiconductors, the insulating behavior is true, since hopping conductivity is related to electron hops between localized states, positioned inside the impurity band. In granular conducting systems, hopping conductivity is related to tunneling hopes of electrons from one metallic granule to neighboring granule. The tunneling is originated from presence of intergranular boundaries.

As was mentioned above, destroying the superconducting state under magnetic field takes place within broad range of the fields (Fig. 4) that is one of specific characteristics of type-II superconductors. For true type-II superconductors, the superconducting state starts destroying at lower critical field, B_{cl}, but complete suppressing superconductivity takes place only at upper critical magnetic field, B_{cu}. Between B_{cl} and B_{cu}, the superconducting and normal phases are coexisting, but a volume ratio between these phases is changed with varying B. Similar critical fields can be introduced to characterize destroying the superconducting state under magnetic field in granular conducting systems. For these systems, individual metallic granules become superconducting at and below B_{cu}, whereas all superconducting granules are coupled at and below B_{cl}. Hence, for granular conducting systems, both the $\rho(T)$ dependence, which corresponds to transition from normal to superconducting state (Fig. 2), and the $\rho(B)$ dependence, which corresponds to transition from superconducting to normal state (Fig. 3), should reflect this two-staged implementation of the superconducting transition. The field B_C in Fig. 4 is obviously related to B_{cu}. The field B_{cl} is very small to be estimated in our experiments.

Thus, all the features of the resistivity superconducting transition found in the samples of single-crystalline 0.95(CdSb)–0.05(NiSb) system are really typical for granular conducting systems. There are reasons to consider these samples as granular conducting systems. As was mentioned above, owing to low solubility of Ni in CdSb lattice, two types of inhomogeneities can be formed in the samples. Besides micro-sized needle-like NiSn crystals (Fig. 1), nano-sized $Ni_{1-x}Sb_x$ clusters can be also formed in Ni-doped CdSb [22]. These inhomogeneities could be responsible for features in the properties, which are characteristic for granular conducting systems. Then, superconductivity in two-component 0.95(CdSb)–0.05(NiSb) system should be attributed to NiSb component. However, no superconductivity has been found in NiSb itself at cooling down to 2 K [23]. Stable CdSb is not superconductor under normal conditions, too [24]. However, superconductivity in alloys of Cd-Sb system could be observed, if these alloys were transformed into a metallic phase by applying high pressure [25]. After this high-pressure treatment, the $Cd_{50}Sb_{20}$ and $Cd_{47}Sb_{53}$ alloys undergo the superconducting transitions at temperatures of 4.6 and 4.5 K, respectively [26, 27]. However, the superconducting state was unstable and fast vanished under thermo-cycling. Instability of the superconducting state is associated with forming amorphous insulating phase during thermo-cycling. The superconducting state found in the $Cd_{0.95}Ni_{0.05}Sb$ sample is stable, and the superconducting transition is repeatable during, at least, 30 processes of thermo-cycling. Besides, the insulating $\rho(T)$ behavior was observed above the superconducting transition. In contrast to the $Cd_{50}Sb_{20}$ and $Cd_{47}Sb_{53}$ alloys prepared via high-pressure treatment, no true metal phase formed in this case. Therefore, the superconducting state observed in CdSb – NiSb system is due to combination and interplay of the physical properties of both CdSb and NiSb, which are usually non-superconducting themselves. Mechanism responsible for superconductivity in this system seems to be related to its inhomogeneity and disorder.

Besides zero electrical resistivity, forming the superconducting transition is usually accompanied by appearance of a diamagnetic response, too. Unfortunately, at present we have no experimental facilities to carry out magnetic measurements. However, the features observed in temperature and magnetic field dependences of the specific electrical resistivity of the sample being studied very well correspond to the resistivity superconducting transition.

4. Conclusion

Thus, superconductivity has been for the first time found in single crystal of two-component 0.99(CdSb)–0.01(NiSb) system. All the features of the resistivity superconducting transition are typical for granular conducting systems.

Declaration of Competing Interest

The authors declare that they have no known competing financial interests or personal relationships that could have appeared to influence the work reported in this paper.

Acknowledgements

This work was supported by the Ministry of Education and Science of the Russian Federation (grant number 0851–2020–0035).

References

[1] B.I. Shklovskii, A.L. Efros, Electronic Properties of Doped Semiconductor, Springer, Berlin, Germany, 1984.
[2] O. Ivanov, M. Yaprintsev, Variable-range hopping conductivity in Lu-doped Bi2Te3, Sol. St. Sci. 76 (2018) 111–117, https://doi.org/10.1016/j.solidstatesciences.2017.12.012.
[3] J. Hu, M.M. Parish, T.F. Rosenbaum, Nonsaturating magnetoresistance of inhomogeneous conductors: comparison of experiment and simulation, Phys. Rev. B. 75 (2007), 214203–1-9, https://doi.org/10.1103/PhysRevB.75.214203.
[4] M.M. Parish, P.B. Littlewood, Classical magnetotransport of inhomogeneous conductors, Phys. Rev. B. 72 (2005), 094417–1-11, https://doi.org/10.1103/PhysRevB.72.094417.
[5] A. Husmann, J.B. Betts, G.S. Boebinger, A. Migliori, T.F. Rosenbaum, M.L. Saboungi, Megagauss sensors, Nature 417 (2002), https://doi.org/10.1038/417421a, 421–1-4.
[6] G.K. van Ancum, M.A.J. Verhoeven, D.H.A. Blank, H. Rogalla, Electric-field activated variable-range hopping transport in PrBa2Cu307-δ, Phys. Rev. B. 52 (1995) 5598, https://doi.org/10.1103/PhysRevB.52.5598.
[7] O. Ivanov, M. Yaprintsev, E. Danshina, Transverse magnetoresistance peculiarities of thermoelectric Lu-doped Bi2Te3 compound due to strong electrical disorder, J. Rare Earths. 37 (2019) 292–298, https://doi.org/10.1016/j.jre.2018.07.007.
[8] M. Mueller, E. Lebanon, History dependence, memory and metastability in electron glasses, J. Phys. IV France. 131 (2005) 167–170, https://doi.org/10.1051/jp4:2005131040.
[9] M. Ben-Chorin, Z. Ovadyahu, M. Pollak, Nonequilibrium transport and slow relaxation in hopping conductivity, Phys. Rev. B. 48 (1995) 15025–15034, https://doi.org/10.1103/PhysRevB.48.15025.
[10] D. Kabiraj, S. Ghosh, Metastability of defects, potential fluctuations, and percolation transition in GaAs, Sol. St. Commun. 149 (2009) 1884–1887, https://doi.org/10.1016/j.ssc.2009.08.008.
[11] Y. Deguchi, H. Kikuchi, N. Mori, Y. Yamada, T. Atsumi, K. Yoshida, T. Ishibashi, Fluctuation-conductivity characterization of superconducting Bi2Sr2CaCu2O8+d thin films prepared by the metal-organic decomposition method, Phys. Proc. 45 (2013) 193–196, https://doi.org/10.1016/j.phpro.2013.04.086.
[12] edited by A.I. Larkin, A.A. Varlamov, Fluctuation Phenomena in Superconductors, in: K.-H. Bennemann, J.B. Ketterson (Eds.), Handbook on Superconductivity: Conventional and Unconventional Superconductors, Springer, Berlin, Germany, 2002. edited by.
[13] I.S. Beloborodov, A.V. Lopatin, V.M. Vinokur, K.B. Efetov, Granular electronic systems, Rev. Mod. Phys. 79 (2) (2007) 469–518, https://doi.org/10.1103/RevModPhys.79.469.
[14] B.D. Tinh, L.M. Thu, AC fluctuation conductivity in type-II superconductors, Mod. Phys. Lett. B. 26 (2012), 1250143–1-4, https://doi.org/10.1142/S0217984912501436.
[15] O.N. Ivanov, A.V. Fokin, Yu.A. Kumzerov, A.A. Naberezhnov, Features of superconducting transition in nanocomposite consisting of “insulating matrix (porous alkali-borosilicate glass)” – “granular metallic filler (indium)”,, Chin. J. Phys. 37 (2020) 376–387, https://doi.org/10.1016/j.cjph.2020.07.003.
[16] Y. Umehara, S. Koda, Structure and phase-boundary energies of the directionally solidified InSb-MnSb-NiSb, InSb-FeSb, and InSb-CrSb eutectic alloys, Metallography 7 (1974) 313–331, https://doi.org/10.1016/0026-0800(74)90012-3.
[17] Y. Pan, G. Sun, Magnetic properties of directionally solidified MnSb/Sbeutectic composite, Scr. Mater. 41 (1999) 803–807, https://doi.org/10.1016/S1359-6462(99)00228-6.
[18] L. Rednic, I. Deac, E. Dorolti, M. Coldea, V. Rednic, M. Neumann, Magnetic cluster developement in In1−x MnxSb semiconductor alloys, Cent. Eur. J. Phys. 8 (2010) 620–627, https://doi.org/10.2478/s11534-009-0140-7.
[19] R. Laiho, A.V. Lashkul, E. Lähderanta, K.G. Lisunov, I. Ojala, V.S. Zakhvalinskii, Magnetic properties of CdSb doped with Ni, J. Magn. Magn. Mater. 300 (2006) e8–e11, https://doi.org/10.1016/j.jmmm.2005.10.137.
[20] S. Matsuo, H. Sugiuro, S. Noguchi, Superconducting transition temperature of aluminum, indium, and lead fine particles, Low. Temp. Phys. 15 (1973) 481–490, https://doi.org/10.1007/BF00654622.
[21] C. Tien, C.S. Wur, K.J. Lin, E.V. Charnaya, Yu.A. Kumzerov, Double-step resistive superconducting transitions of indium and gallium in porous glass, Phys. Rev. B. 61 (2000) 14833–14838, https://doi.org/10.1103/PhysRevB.61.14833.
[22] R. Laiho, A.V. Lashkul, K.G. Lisunov, E. Lähderanta, I. Ojala, V.S. Zakhvalinskii, The influence of Ni-rich nanoclusters on the anisotropic magnetic properties of CdSb doped with Ni, Semicond. Sci. Technol. 21 (2006) 228–235, https://doi.org/10.1088/0268-1242/21/3/003.
[23] X.-N. Luo, D. Cheng, S.-K. Liu, Z.-P. Zhang, A.-L. Li, L.-H. Yang, X.-C. Li, Low-temperature physical properties and electronic structures of Ni3Sb, Ni5Sb2, NiSb2, and NiSb, Chin. Phys. B. 24 (2015), 067201–1-6, https://doi.org/10.1088/1674-1056/24/6/067201.
[24] H. Matsunami, Y. Nishihara, T. Tanaka, Electrical properties of undoped p-CdSb at low temperatures, J. Phys. Soc. Jpn. 27 (1969) 1507–1516, https://doi.org/10.1143/JPSJ.27.1507.
[25] V.F. Gantmakher, V.N. Zverev, V.M. Teplinskii, G.E. Tsydynzhapov, O.I. Barkalov, Anomalous superconducting response and nonactivating tunneling in high-resistance metastable states of GaSb, JETP 77 (1993) 513–520. http://www.jetp.ac.ru/cgi-bin/dn/e_077_03_0513.pdf.
[26] V.F. Gantmakher, V.M. Teplinskii, V.N. Zverev, O.I. Barkalov, Interplay of superconducting and insulating phases in the metastable high-resistance states of the Ga50Sb50 alloy, Physica B 194-196 (1994) 1085–1086, https://doi.org/10.1016/0921-4526(94)90872-9.
[27] V.F. Gantmakher, V.M. Teplinskii, V.N. Zverev, O.I. Barkalov, Superconducting response in bulk CdSb alloy near the localization threshold, Physica B 194-196 (1994) 1083–1084, https://doi.org/10.1016/0921-4526(94)90871-0.